Identification and analysis of large paleo-landslides at Mount Burnaby, British Columbia

Mirko Francioni [a], Doug Stead [b], John J. Clague [b], Allison Westin[b]

[a] Camborne School of Mines, University of Exeter, Cornwall, United Kingdom

[b] Department of Earth Sciences, Simon Fraser University, Vancouver, BC, Canada

Abstract

This paper presents a multi-scale and multidisciplinary study of large, late Pleistocene or early Holocene slumps in Eocene sedimentary rocks at Mount Burnaby, just east of Vancouver, British Columbia (BC). Airborne LiDAR and field data were integrated into a GIS to understand the origin, kinematics, and subsequent history of the landslides. Products derived from the bare-earth LiDAR data include an engineering geomorphology map, shaded relief maps, and several LiDAR slope profiles. To understand the landslides better, we analyzed discontinuities and structural lineaments. The structure of the Eocene rocks underlying Mount Burnaby was compared with trends of local lineaments, and the shape of the coastline of Burrard Inlet and Indian Arm, and trends of regional faults and lineaments identified by previous researchers working in southwest BC. Two main joint systems likely played a key role in conditioning the north slope of Mount Burnaby for failure. The landslides probably happened during or soon after deglaciation of the area at the end of the Pleistocene on the steep north face of Mount Burnaby after a 200-m fall in relative sea level caused by glacio-isostatic uplift of the crust.

Keywords

Paleo-landslides, LiDAR, GIS, Engineering geomorphology

1 Introduction

In this paper, we document a previously unknown complex of large slumps in the Vancouver, British Columbia (BC), metropolitan area. The slumps, which occurred on the steep north face of Mount Burnaby at the edge of Simon Fraser University, are the largest known mass movement in south-coast British Columbia. We were able to document and infer the cause of the landslides through an integrated study involving field mapping, new LiDAR imagery, and data analysis within a multi-layered GIS.

The slumps are probably of late Pleistocene or early Holocene age, but given their size, questions arise about whether or not similar landslides might occur in the future. If this were to happen, parts of Simon Fraser University and an allied community (UniverCity), as well as a railway and highway at the base of Mount Burnaby might be damaged.

Acquisition of a LiDAR point cloud of Mount Burnaby provided an opportunity to create thematic maps, slope profiles, and an engineering geomorphological map that enabled an interpretation of the geometry

and original positions of slump blocks and sites subject to reactivation that could damage public works. In this paper, we describe the multi-disciplinary approach we used to identify and characterize the slumps. We also characterize the local and regional structural environment in which the slumps occurred, and consider how likely it is that a similar slope failure might happen in the future.

1.1 Study area

Mount Burnaby is a small forested mountain (peak elevation 350 m asl) located approximately 10 km east of Vancouver, BC, and just south of Burrard Inlet (Figure 1A). Simon Fraser University (SFU), which opened in 1965, is situated at the top of the mountain.

The mountain is a remnant of formerly more extensive Eocene terrestrial sedimentary rocks that are part of a Cretaceous-Cenozoic fill in the Georgia Basin, which lies between the Coast Mountains to the north, the spine of Vancouver Island to the west, and the Cascade Range in Washington State, USA, to the southeast (Armstrong 1990; Mustard and Rouse 1994; Turner et al. 1998). The rocks consist of conglomerate, sandstone, and mudstone of alluvial and deltaic origin deposited in a subsiding structural basin. There are few natural exposures of the rocks on Mount Burnaby, but the same sequence of rtocks is commonly exposed in building excavations in downtown Vancouver.

Mount Burnaby has a pronounced asymmetric north-south profile, reflecting the ca. 11° southerly dip of the entire Eocene sequence (Figure 1B). A south-thickening wedge of Fraser Glaciation till and glaciomarine sediments overlies the inclined bedrock surface on the southerly dip slope (Armstrong 1990; Roddick 1965). The glacial sediments partially, but not completely, mask the underlying bedrock structure. A series of steps on the south-facing slope, which are only evident in LiDAR images, reflect daylighting beds of sandstone, conglomerate, and mudstone that have different resistances to erosion. In contrast, the forest-covered north slope of the mountain is very steep and, for this reason, has not been studied in the past.

2 Methods

Several tasks were completed to understand the geology of Mount Burnaby better. Specifically, we created thematic maps and slope profiles, produced an engineering geomorphology map, identified major structural lineaments visible in the LiDAR data, and analyzed coastline trends to determine if they might be structurally controlled. The results were validated and integrated with stratigraphic and structural data acquired through fieldwork. We pinpointed areas where relict slump blocks are prone to re-activation due to human activity and, finally, compiled all data in a GIS database to interpret, visualize, and share the data. Figure 2 is a flow chart summarizing the methodology used in this study.

2.1 LiDAR and GIS analyses

Airborne LiDAR data for the area shown in Figure 3A were provided in LASer (LAS) file format and processed using the GIS software ESRI's ArcMap version 10.2. LAS was created and is maintained by the American Society for Photogrammetry and Remote Sensing (ASPRS); it is a standard file format for the exchange of LiDAR data. Each LAS file contains records of all laser pulses recorded. The first returns are typically associated with the highest features in the landscape, for example a treetop or the top of a building, whereas the last return is from the ground surface. In this research, we filtered out all but the last

returns to produce a bare-earth layer, from which we built a 1-m-resolution DTM (digital terrain model) of the mountain. Numerous authors have discussed the use of GIS in landslide and structural geology investigations (e.g., Van Westen 1998; Xie et al. 2006; Francioni et al. 2014, 2015).

We produced and used three main thematic maps: hillshade, slope, and aspect (respectively Figure 3B-D). A hillshade map (Figure 3B) was generated using a lighting effect based on differences in elevation within the landscape. It provides synthetic three-dimensional views of the landscape. The light angle used in Figure 3B has an azimuth of 315° (light cast from the northwest) and an inclination of 25°. The slope map (Figure 3C) shows the steepness of the slopes. The aspect map (Figure 3D) shows the dip direction of slopes and was used in this study to highlight abrupt changes in slope orientation.

2.2 Engineering geomorphology map and slope profiles

We produced an engineering geomorphology map (presented and described in section 3 of this paper) of the north side of Mount Burnaby using guidelines in Cooke and Doornkamp (1990). We mapped: i) linear terrain features, including concave and convex slopes, cliffs (terrain steeper than 45°), lineaments, and gullies; and ii) landforms including debris flow fans and slump blocks. Faults, bedding, and joints were represented as point values on the map. We also created topographic profiles across the north, west, and south sides of Mount Burnaby to characterize its topography and geometry better.

2.3 Structural analysis

We measured trends of lineaments on Mount Burnaby (red lines in Figure 4). In addition, we measured conspicuous linear sections of the coastlines of Burrard Inlet and Indian Arm in the vicinity of the mountain (blue lines in Figure 4) to determine if their geometries might be structurally controlled and in agreement with the lineaments on the mountain. The same approach was also used to measure the average orientations of mapped faults in southwest BC (British Columbia Ministry of Energy and Mines 2014) (Figure 5).

2.4 Field survey

All natural and man-made exposures on Mount Burnaby were documented to obtain as much information as possible about the stratigraphy and structure of the mountain. Due to the presence of dense vegetation and the inaccessibility of most of the steep north slope of the mountain, we could only document 11 outcrops in the area (Figure 6A). Figure 6B shows an example of geological characterization of one of the outcrops (SFU2). The orientations of all discontinuities and faults exposed in outcrops were measured. Finally, we also examined borehole logs and reports provided by BGC Engineering, which include geotechnical information on foundation conditions at Simon Fraser University.

2.5 Geodatabase and data sharing

We developed a GIS database to manage the thematic maps, shape files, and field data (outcrop locations and observations, and structural elements). LiDAR maps and Google Earth were used as base maps; through hyperlinks it was possible to electronically link information to specific sites. The GIS was also an important resource for sharing data with others, using the freeware platform ArcReader (ESRI 2014) and Google Earth (2015).

3 Results

We rendered 3D visualizations of the 2D thematic maps, such as those shown in Figure 3B-D to identify and interpret the paleo-landslides on the north side of Mount Burnaby. Figure 7 is an example of a 3D representation of the aspect map that clearly shows back-tilted slump blocks on the north side of the mountain. The faces of the back-tilted slump blocks are approximately parallel to the headscarp, indicating that they detached from that area.

Figure 8 illustrates the difference between the steep north face of Mount Burnaby, with slopes typically ranging from 40° to 80°, and the much gentler south face inclined 5-15°, reflecting the ca. 11° southerly dip of the Eocene sequence. The main gully that indents the north face of the mountain marks the border between two different slope environments. East of the gully, a gentle, north-dipping slope separates the top of the mountain from the steep landslide headscarp, whereas to the west, the mountain top abruptly borders the steep north slope.

Barnet Highway extends across the toes of some of the slumps blocks (Figures 7 and 8). Since construction of the highway in the early 1940s, there have been small slope failures at its margins, which we attribute to reactivation of the slump blocks.

Figures 9 and 10 show the engineering geomorphology map of Mount Burnaby. We separated the north side of the mountain into two areas to highlight geomorphic and geological features (Figure 9). Area 1 (Figure 10A) contains 14 slump blocks that are partially covered by fan deposits and might be connected to one another below the surface. All fan deposits slope away from the cliff face. All except one of the convex breaks of the slump blocks align with the cliff face, indicating their source and supporting the interpretation drawn from the aspect map. Area 2 (Figure 10B) contains four slump blocks, one on the north side of Barnet Highway and the other three south of the highway. The convex breaks in these blocks align and are approximately parallel to the cliff face.

Numerous steep gullies extend down the north slope of the mountain. The largest gully, located at northwest corner of Simon Fraser University (Figure 3B), has a northeast trend and a gradient ranging from 40° to 85°; it has retrogressed towards the south much more that other gullies.

Representative slope profiles on the north, west, and south sides of the mountain were used to highlight geomorphic features and slope geometries (Figure 11A). Profiles of the north slope show its steep upper face and the presence and geometry of the slump blocks (Figure 11B). The west slope has a series of topographic steps reflecting the alternation of sandstone, conglomerate, and mudstone units with different resistances to erosion (Figure 11C). The steps are up to about 10 m high, have average gradients of 14-24°, and are separated by treads with gradients of 3-6°. The slope on the south side of the mountain is much more gentle, reflecting the ca. 11° southerly dip of the entire Eocene sequence (Figure 11D).

Several lines of evidence reveal two main sets of structures, both throughout the region and on and near Mount Burnaby (Figure 12). First, regional faults extracted from the databases of the British Columbia Ministry of Energy and Mines strike northeast-southwest (ca. N 046°) and northwest-southeast (ca. N 125°) (Figure 12A). Second, the shorelines of Burrard Inlet and Indian Arm are rectilinear, with ca. N

045° and N 125° trends (Figures 4 and 12B). Third, lineaments evident on thematic maps trend ca. N 55° and N 145° (Figure 12C). Together, the two sets delineate the bimodal geometry of crest of the escarpment on the north side of the mountain (Figure 4). Fourth, field measurements of fractures and faults confirm these two main sets on an outcrop scale – one striking about 055° and the other 135° (Figure 12D). Although there is strong structural control on the geomorphology of the mountain, we found no evidence that any of the structures are currently active.

Field observations indicate that the exposed Eocene rocks are highly weathered rock and dense soils, mainly of sand and gravel size. Using field techniques (Hoek and Brown 1997), we estimated the strength of these rocks is estimated to be between 1 and 5 MPa. Rock cores recovered in four boreholes recently drilled by BGC Engineering yielded Uniaxial Compressive Strength values of 19 MPa for mudstone, 10 MPa for sandstone, and 18 MPa for conglomerate (Schmid and Baumgard 2014). The difference between unconfined compressive strengths of the deep rocks and those at the surface is due to weathering, which has leached cement and matrix from rock in the near-surface environment (Clague et al. 2015).

Figure 13 shows the result of a slope profile analysis that helped us to define the geometry of the paleo-landslides and interpret the failure mechanism better. Slope profile D-D' (Figures 13A and 13B) shows three slump blocks sourced on the steep headwall of the mountain to the south. The headscarp reaches an elevation of 200 m asl and has an average gradient of 51° towards the northwest. The slump block closest to the headwall, which is the youngest of the three, has a back-tilted face dipping 38° parallel to the headscarp. The base of the back-tilted face is about 100 m below the top of the headscarp and about 215 m away from it. The other two, older slump blocks are about 110 m and 160 m below the top of the headscarp and 330 m and 585 m away from it. Again, the slump blocks are parallel to the headscarp and dip backward at 12° and 18°. Slope profile E-E' (Figure 13C) shows two slump blocks 190 m and 220 m below the top of the headscarp (270 m asl) and 475 m and 645 m from it. The headscarp has an average gradient of 60°. The slump blocks dip 32° and 15° towards the headscarp. Slope profile F-F' (Figure 13D) shows a single slump block 190 m below the top of the headscarp (230 m asl) and 460 m from it. The headscarp has an average gradient of 65°. This slump block dips 20° towards the headscarp.

Figure 14 illustrates a possible failure mechanism for the landslides based on the maps produced in this study. Measurements made using LiDAR slope profiles and the thematic maps allowed us to calculate the length, width, and angle of the back-tilted face of the uppermost slump block (respectively 250 m, 50 m, and 38°). Assuming that the surface of Mount Burnaby extended to the north beyond the headscarp with a gradient similar to that of the present surface, we conclude that a block failed along a curved surface and rotated 38° before coming to rest. We note, however, that post-landslide fan deposits partially envelop the slump block, introducing uncertainties in our estimates of block dimensions and volume. Considering the similarities in the geometry and orientation of all slump blocks on north side of the mountain (Figure 9), we assume that the blocks were generated by the same failure mechanism.

The many gullies incising the north slope are evidence of the relative ease with which the sedimentary rocks underlying the mountain are eroded. The main gully is likely located on a northeast-southwest structure, possibly a fault, along which there has been enhanced erosion. Erosion along this and other northeast-trending lineaments may have favoured the formation of lateral relief surfaces for the landslide.

4 Discussion

Airborne LiDAR is now widely used in landslide studies (e.g., Chen et al. 2006; Ventura et al. 2011; Brideau et al. 2012; Haas et al. 2012) because it provides detailed georeferenced 3D models of the land surface free of vegetation. In this paper, we feature the symbiotic integration of airborne LiDAR with GIS techniques in a study of the Mount Burnaby paleo-landslide, as has been done successfully by other landslide researchers in the past (Schulz 2007; Van Den Eeckhaut et al. 2012; Jebur et al. 2014).

The information obtained from the thematic maps and LiDAR interpretation were used to produce an engineering geomorphology map of Mount Burnaby that could not otherwise have been made. This map and the aspect map allowed us to define the position and geometry of the slump blocks and to suggest their source and movement direction. Analysis of the engineering geomorphology map showed that fan deposits overlie the slump blocks and are derived from the same source, but clearly postdate them.

LiDAR data were also critical for analysing Mount Burnaby slope profiles, which aided in understanding the geometry of the mountain and the paleo-landslides. The steps reflecting the alternation of layers of sandstone, conglomerate, and mudstone could not be seen in conventional aerial photographs and only became obvious when we examined the LiDAR DEM. The slope profiles also supported the interpretation of the geometry and source of the slump blocks.

Our analysis highlighted two main discontinuity systems that are likely a product of Paleogene or Neogene tectonic deformation. Although we found no evidence of active (Holocene) faults in the area, the consistent structure at all scales suggests that deformation related to these two main trends played an important role in the evolution of both Mount Burnaby and Burrard Inlet. Lineaments with these trends also define the main scarp and the main gully on the mountain.

The presence on the north side of Mount Burnaby of multiple slump blocks with similar geometries and orientations (Figure 11 and 13) suggests a series of retrogressive events that were closely spaced in time. Although we were unable to determine the exact ages of the landslides, the large volume of fan material overlying the slump blocks suggests that the failures happened during late Pleistocene or early Holocene time, either during local deglaciation or shortly thereafter. The Vancouver area, including Mount Burnaby was deglaciated about 13,500 years ago (Clague 1981); at that time relative sea level was about 200 m higher than today and only the upper slopes of Mount Burnaby were above the sea surface (Mathews et al. 1970; Clague et al. 1982). Shortly after deglaciation, and by no later than 11,000 years ago, glacio-isostatic rebound rapidly lowered local sea level to below its present datum. Glacier retreat and glacio-isostatic rebound may have contributed to the massive slope failures on the north side of Mount Burnaby. The importance of glacier debuttressing as a cause of slope failure has been highlighted by Evans and Clague (1994). Removal of ice confinement allows for kinematic failure, while the fall in sea level due to rebound may have been accompanied by increased erosion of the toe of the slope. Earthquakes caused by glacio-isostatic rebound may also be implicated in the landslides.

Recognition of the landslides on Mount Burnaby has raised concerns over the possibility that similar failures in the densely populated Vancouver metropolitan area could happen in the future. In our view, however, the Mount Burnaby slumps occurred in response to processes that no longer affect this area,

223 namely deglaciation and large and rapid sea-level change. Therefore, we consider it unlikely that a slump
224 like the ones we have documented will happen again in the Vancouver area.

225 ## 5 Conclusion

226 Mount Burnaby consists of several hundred metres of Eocene sandstone, conglomerate, and mudstone
227 that dip about 11° to the south. The gently dipping south slope of the mountain is mantled by a
228 southward-thickening wedge of Pleistocene glacial and glaciomarine sediments. The surface Eocene
229 rocks are highly weathered and typically have the strength of soils (as the term is used in an engineering
230 sense of the word). Non-weathered rocks at depth have unconfined compressive strength properties
231 characteristic of indurated sedimentary rocks.

232 Our integrated study of LiDAR-derived thematic maps, slope profiles, a derived engineering
233 geomorphological map, and field observations show that the north slope of Mount Burnaby failed as a
234 series of large slump blocks that are now partially buried by coalescent debris flow fans sourced on the
235 steep slope to the south. Although the slump blocks at the base of the mountain are relicts of latest
236 Pleistocene or early Holocene landslides, they have spawned small reactivation failures along Barnet
237 Highway over the past 60 years. The identification of these previously unrecognized landslides is
238 significant in showing the power of a modern, integrated approach for analyzing the land surface, as well
239 as the implications that they can carry for managing landslide hazards in urban areas. We advocate the use
240 of thematic and engineering geomorphology maps to identify landslides prior to construction or
241 improvement of private and public infrastructure.

242 Our LiDAR-assisted interpretation of structural trends helped document two main fracture and fault sets,
243 one oriented NW-SE and the other NE-SW. Paleogene or Neogene deformation responsible for these joint
244 sets played a key role in creating the present landscape of the Vancouver metropolitan area. Field study
245 and an examination of LiDAR imagery revealed no evidence of Holocene faulting in the area, although
246 the limited exposure of rock on Mount Burnaby does not allow us to definitively preclude this possibility.

247 ## 6 Acknowledgments

248 We are grateful to BGC Engineering for its support of our research, and in particular acknowledge Alex
249 Baumgard, who helped us secure LiDAR imagery and funding that allowed us to undertake the project.
250 The research was supported with grants provided by Kinder Morgan Canada and the Natural Sciences and
251 Engineering Research Council of Canada (NSERC Discovery Grants to ds and jjc). Three journal
252 reviewers (Kim Bishop, Keith Loague, and one anonymous referee) provided critiques that allowed us to
253 improve the paper.

254 ## 7 References

255 ADAM Technology. 2014. 3DM Analyst and Calibcam. http://www.adamtech.com.au.

256 Armstrong, J.E. 1990. Vancouver Geology. Geological Association of Canada, Cordilleran Section,
257 Vancouver, BC, 128 pp.

Brideau, M.A., Sturzenegger, M., Stead, M., Jaboyedoff, M., Lawrence, M., Roberts, N.J., Ward, B.C., Millard, T.H., Clague, J.J. 2012. Stability analysis of the 2007 Chehalis lake landslide based on long-range terrestrial photogrammetry and airborne LiDAR data. Landslides 9: 75-91.

British Columbia Ministry of Energy and Mines. 2014. BC Digital Geology Data http://www.empr.gov.bc.ca/Mining/Geoscience/BedrockMapping/Pages/BCGeoMap.aspx.

Chen, R.F., Chang, K.J., Angelier, J., Chan, Y.C., Deffontaines, B., Lee, C.T., Lin, M.L. 2006. Topographical changes revealed by high-resolution airborne LiDAR data: The 1999 Tsaoling landslide induced by the Chi-Chi earthquake. Engineering Geology 88: 160–172.

Clague, J.J. 1981. Late Quaternary Geology and Geochronology of British Columbia, Part 2: Summary and Discussion of Radiocarbon-dated Quaternary History. Geological Survey of Canada, Paper 80-35, 41 pp.

Clague, J.J., Harper, J.R., Hebda, R.J., Howes, D.E. 1982. Late Quaternary sea levels and crustal movements, coastal British Columbia. Canadian Journal of Earth Sciences 19: 597-618.

Clague J.J., Stead D., Francioni M., Westin A. 2015. Geology of Mount Burnaby. Unpublished report for Kinder Morgan, Calgary, AB.

Cooke, R.U., Doornkamp, J.C. 1990. Geomorphology in Environmental Management: A New Introduction. Clarendon Press, Oxford University Press, New York, Oxford, 434 pp.

Dominion of Canada. 1859. Burrard Inlet [map]. Dominion of Canada; surveyed by Mr. W.J. Stewart, under the direction of Staff Commander J.G. Boulton, R.N. http://searcharchives.vancouver.ca/burrard-inlet-6, accessed September 19, 2014.

ESRI. 2014. ArcMap, ArcReader and ArcScene Version 10.2. http://www.arcgis.com.

Evans, S.G., Clague, J.J. 1994. Recent climatic change and catastrophic geomorphic processes in mountain environments. Geomorphology 10: 107-128.

Francioni, M., Salvini, R., Stead, D., Litrico, S. 2014. A case study integrating remote sensing and distinct element analysis to quarry slope stability assessment in the Monte Altissimo area, Italy. Engineering Geology 183: 290-302.

Francioni, M., Salvini, R., Stead, D., Giovannini, R., Riccucci, S., Vanneschi, C., Gullì, D. 2015. An integrated remote sensing-GIS approach for the analysis of an open pit in the Carrara marble district, Italy: Slope stability assessment through kinematic and numerical methods. Computers and Geotechnics 67: 46-63.

Google Earth. 2015. DigitalGlobe 2012. http://www.earth.google.com.

Haas, F., Heckmann, T., Wichmann, V., Becht, M. 2012. Runout analysis of a large rockfall in the Dolomites/Italian Alps using LIDAR derived particle sizes and shapes. Earth Surface Processes and Landforms 37: 1444-1455.

Hoek, E., Brown, E.T. 1997. Practical estimates of rock mass strength. International Journal of Rock Mechanics and Mining Sciences 34: 1165-1186.

Jebur, M.N., Pradhan, B., Tehrany, M.S. 2014. Optimization of landslide conditioning factors using very high-resolution airborne laser scanning (LiDAR) data at catchment scale. Remote Sensing of Environment 152: 150-165.

Mathews, W.H., Fyles, G., Nasmith, H. 1970. Postglacial crustal movements in southwestern British Columbia and adjacent Washington State. Canadian Journal of Earth Sciences 7: 690-702.

Mustard, P.S, Rouse, G.E. 1994. Stratigraphy and evolution of Tertiary Georgia basin and subjacent Upper Cretaceous sedimentary rocks, southwestern British Columbia and northwestern Washington State. In: Geology and Geological Hazards of the Vancouver Region, Southwestern British Columbia, J.W.H. Monger (ed.). Geological Survey of Canada, Bulletin 481: 97-169.

Rocscience, 2014. Dips Version 6.016. https://www.rocscience.com.

Roddick, J.A. 1965. Vancouver North, Coquitlam and Pitt Lake Map Areas, British Columbia, with Special Emphasis on the Evolution of the Plutonic Rocks. Geological Survey of Canada Memoir 335, http://geogratis.gc.ca/api/en/nrcan-rncan/ess-sst/0062e577-e050-593c-a248-2ddc421744f8.html#distribution.

Schmid, C., Baumgard, A. 2014. Trans Mountain Pipeline ULC, TMEP Westridge Tunnel Investigation. 2014. Site Investigation Data Report. BGC Technical Report, Project No. 0095-150-15, 40 pp.

Schulz, W.H. 2007. Landslide susceptibility revealed by LIDAR imagery and historical records, Seattle, Washington. Engineering Geology 89: 67-87.

Turner, R.J.W., Clague, J.J., Groulx, B.J., Journeay, J.M. 1998. GeoMap Vancouver, Geological Map of the Vancouver Metropolitan Area. Geological Survey of Canada Open File 3511.

Van den Eeckhaut, M., Kerle, N., Poesen, J., Hervás J. 2012. Object-oriented identification of forested landslides with derivatives of single pulse LiDAR data. Geomorphology 173-174: 30-42.

Van Westen, C.J., 1998. GIS in landslide hazard zonation: A view, with cases from the Andes of Colombia, in: Mountain Environment and Geographic Information Systems, F.P. Martin, D.I. Heywood (eds.). Taylor & Francis, London, pp. 35–165.

Ventura, G., Vilardo, G., Terranova, C., Bellucci Sessa, E. 2011. Tracking and evolution of complex active landslides by multi-temporal airborne LiDAR data: The Montaguto landslide (southern Italy). Remote Sensing of Environment 115: 3237-3248.

Xie, M., Esaki, T., Qiu, C., Wang C.X. 2006. Geographical information system-based computational implementation and application of spatial three-dimensional slope stability analysis. Computers and Geotechnics 33: 260-274.

Figure Captions

Figure 1. Mount Burnaby (Google Earth 2015). A) Location of Mount Burnaby in the Vancouver metropolitan area (the inset shows the location of the study area in western Canada). B) 3D view of Mount Burnaby and Simon Fraser University, situated at the top of the mountain. View to the southeast.

Figure 2. Flow chart showing steps followed in the Mount Burnaby study.

Figure 3. Mount Burnaby thematic maps (reference system: NAD 83 Zone 10N, Simon Fraser University as reference). A) Satellite image (Google Earth 2015) showing the area where LiDAR and GIS analyses were carried out. B) Hillshade map. C) Slope map. D) Aspect map.

Figure 4. Mount Burnaby lineaments (red lines) interpreted from thematic maps and linear shoreline segments (blue lines; Dominion of Canada 1859).

Figure 5. Faults in southwest BC (from British Columbia Ministry of Energy and Mines 2014).

Figure 6. A) Hillshade map showing locations of investigated outcrops and boreholes. B) Exposure at SFU 2 (shovel for scale). C, conglomerate; SS, sandstone; M, mudstone.

Figure 7. 3D representation of aspect map with back-tilted slump blocks on the north face of Mount Burnaby, road cuts, and inferred slump headscarp.

Figure 8. 3D representation of the slope map.

Figure 9. Engineering geomorphology map of Mount Burnaby.

Figure 10. Engineering geomorphology maps of (A) area 1 and (B) area 2 (see Figure 9).

Figure 11 Slope profiles. A) Locations of slope profiles shown in B), C), and D). B) Slope profile A-A'. C) Slope profile B-B'. D) Slope profile C-C'.

Figure 12. Rose diagrams showing the results of all structural analyses (rose diagrams created using DIPS [Rocscience 2014]). A) Regional faults. B) Shoreline segments. C) GIS lineaments. D) Faults and fractures measured in the field.

Figure 13. Slope profiles and paleo-landslide geometry. A) Slope map showing the locations of three profiles across the north slope of Mount Burnaby. B) Slope profile D-D'. C) Slope profile E-E'. D) Slope profile F-F'.

Figure 14. A possible failure interpretation for paleo-landslides on the north slope of Mount Burnaby. The slump block used in this example has a length of 250 m and a 50-m back-tilted face.

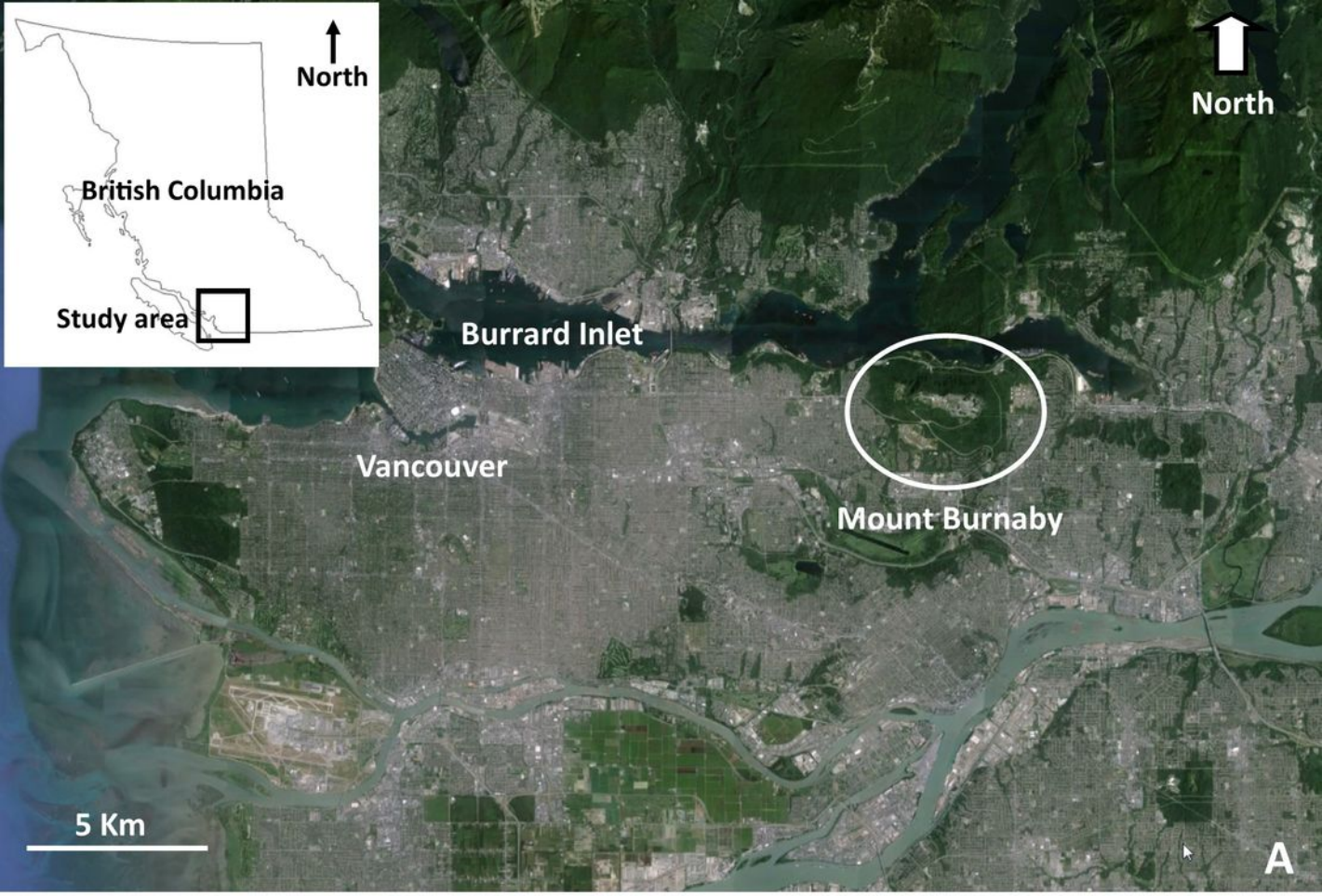
North
British Columbia
Study area
North
Burrard Inlet
Vancouver
Mount Burnaby
5 Km
A


0.6 Km
North
Simon Fraser University
Burrard Inlet
Mount Burnaby
0.6 Km
B

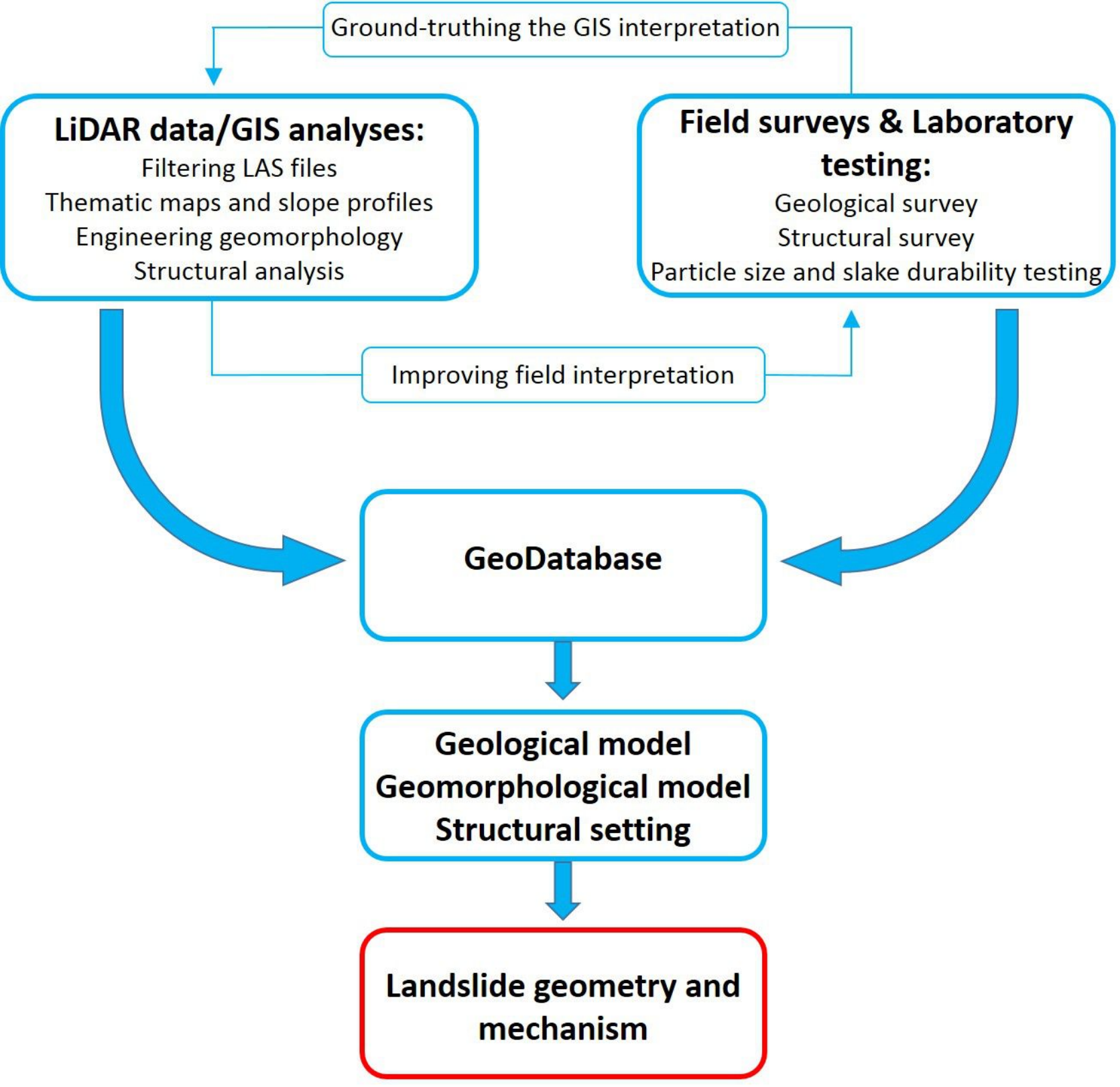
Ground-truthing the GIS interpretation
LiDAR data/GIS analyses:
Filtering LAS files
Thematic maps and slope profiles
Engineering geomorphology
Structural analysis
Field surveys & Laboratory testing:
Geological survey
Structural survey
Particle size and slake durability testing
Improving field interpretation
GeoDatabase
Geological model
Geomorphological model
Structural setting
Landslide geometry and mechanism

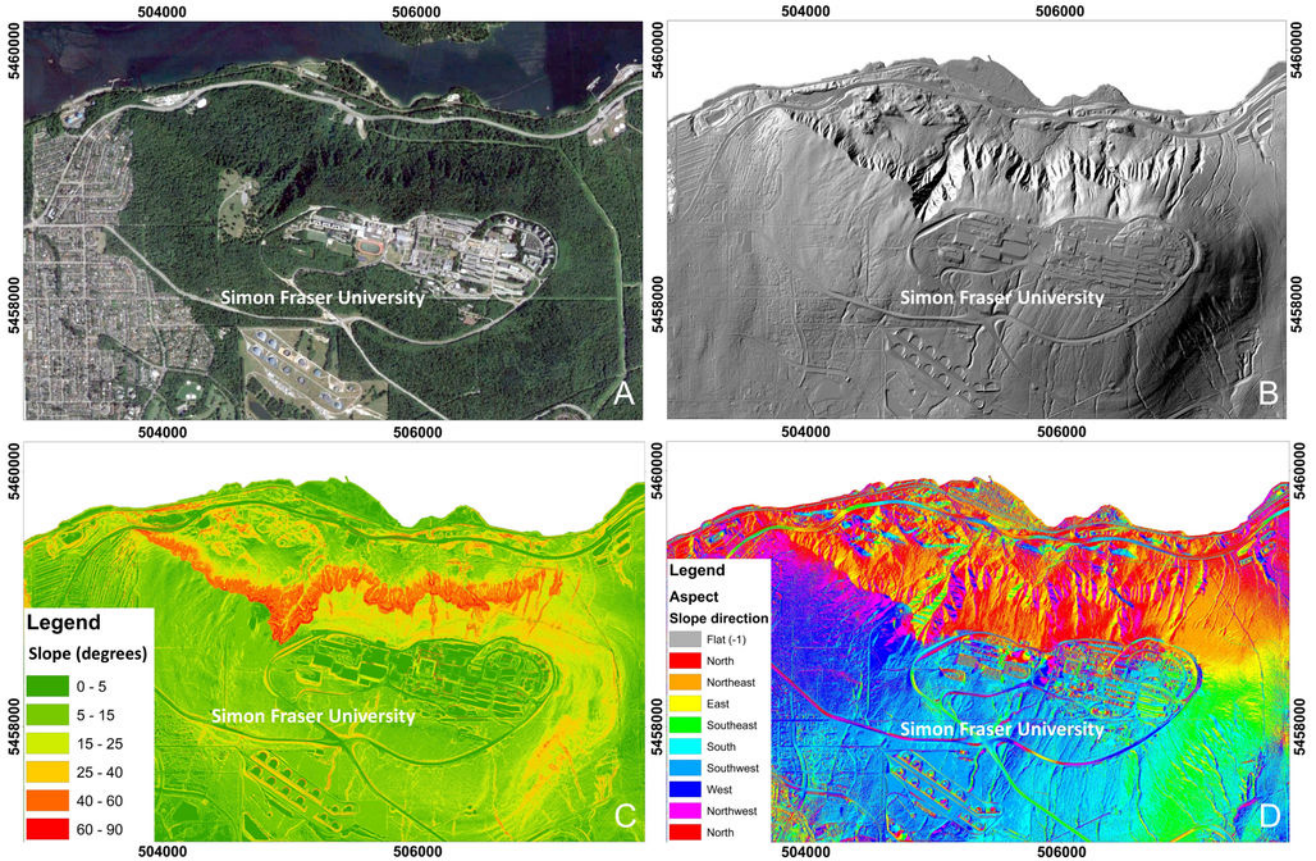
504000
506000
5460000
5458000
Simon Fraser University
A
B
C
D
Legend
Slope (degrees)
0 - 5
5 - 15
15 - 25
25 - 40
40 - 60
60 - 90
Legend
Aspect
Slope direction
Flat (-1)
North
Northeast
East
Southeast
South
Southwest
West
Northwest
North

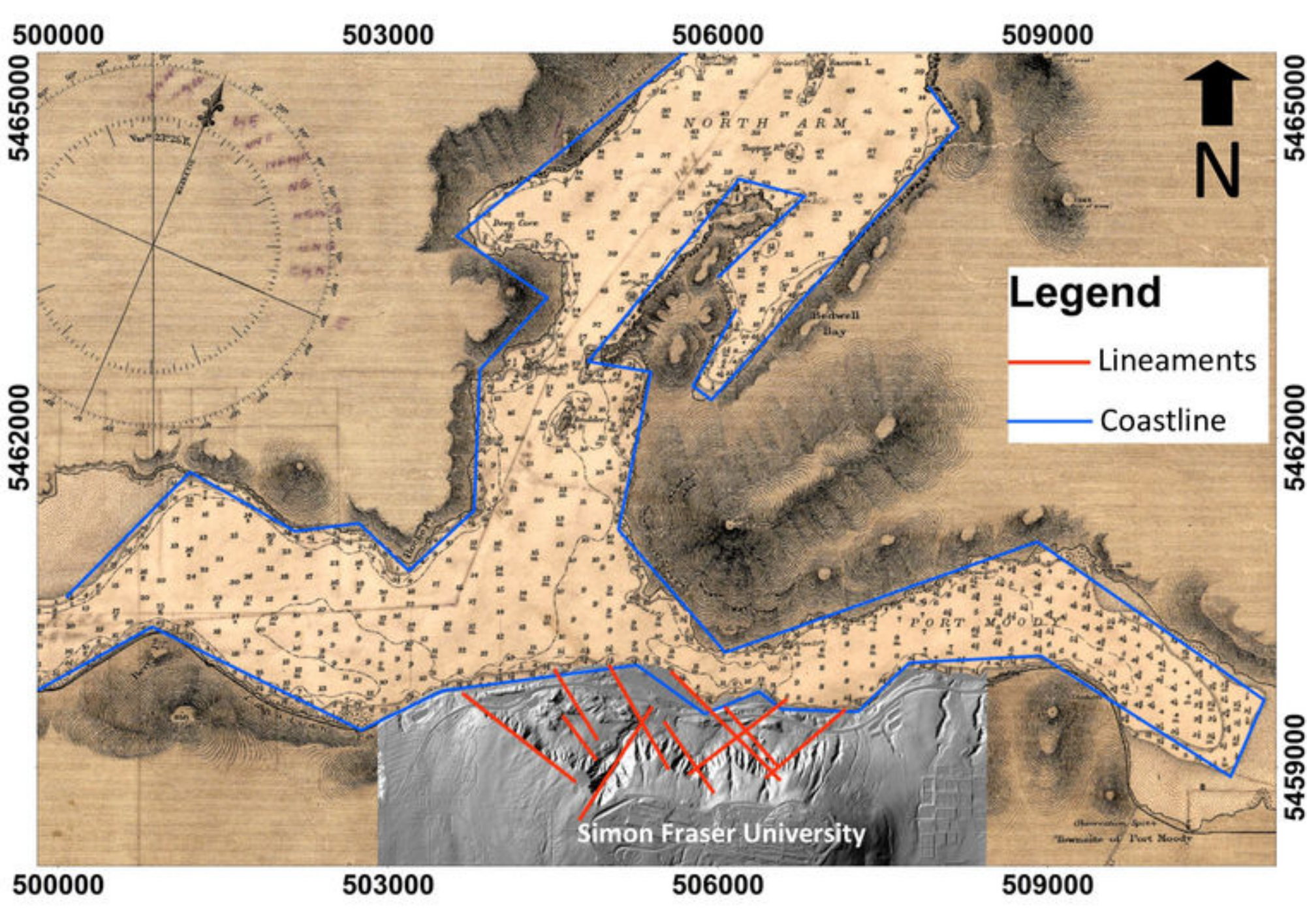
500000
503000
506000
509000
5465000
5462000
5459000
N
NORTH ARM
Bedwell Bay
PORT MOODY
Simon Fraser University
Legend
Lineaments
Coastline

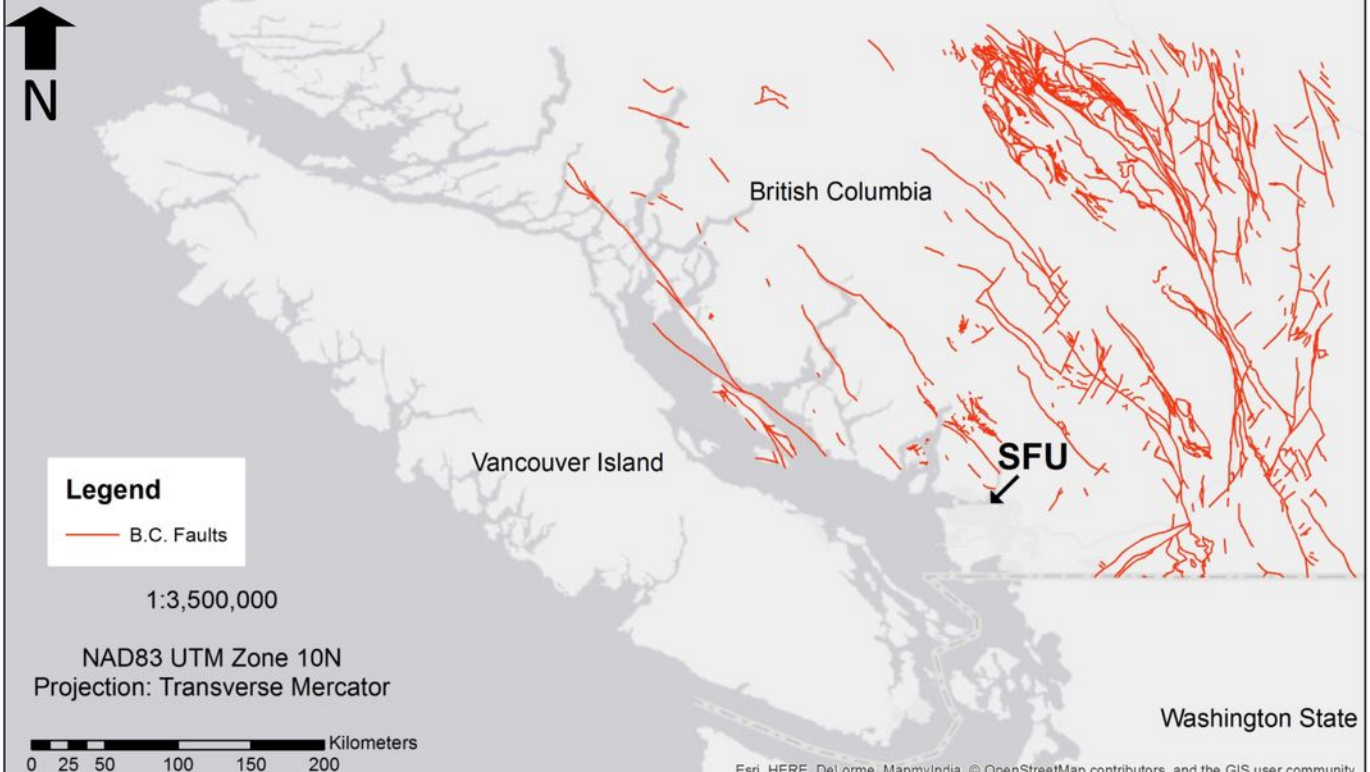
N
British Columbia
Vancouver Island
SFU
Legend
B.C. Faults
1:3,500,000
NAD83 UTM Zone 10N
Projection: Transverse Mercator
Kilometers
0 25 50 100 150 200
Washington State
Esri, HERE, DeLorme, MapmyIndia, © OpenStreetMap contributors, and the GIS user community

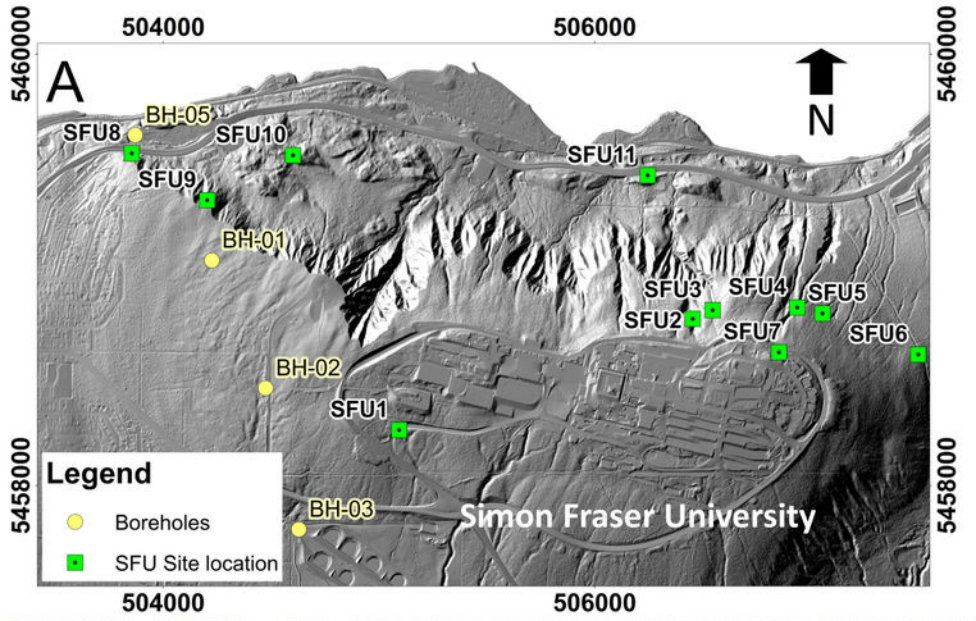
A
504000
506000
5460000
5458000
N
SFU8
BH-05
SFU10
SFU9
SFU11
BH-01
SFU3
SFU4
SFU5
SFU2
SFU7
SFU6
BH-02
SFU1
BH-03
Simon Fraser University
Legend
Boreholes
SFU Site location

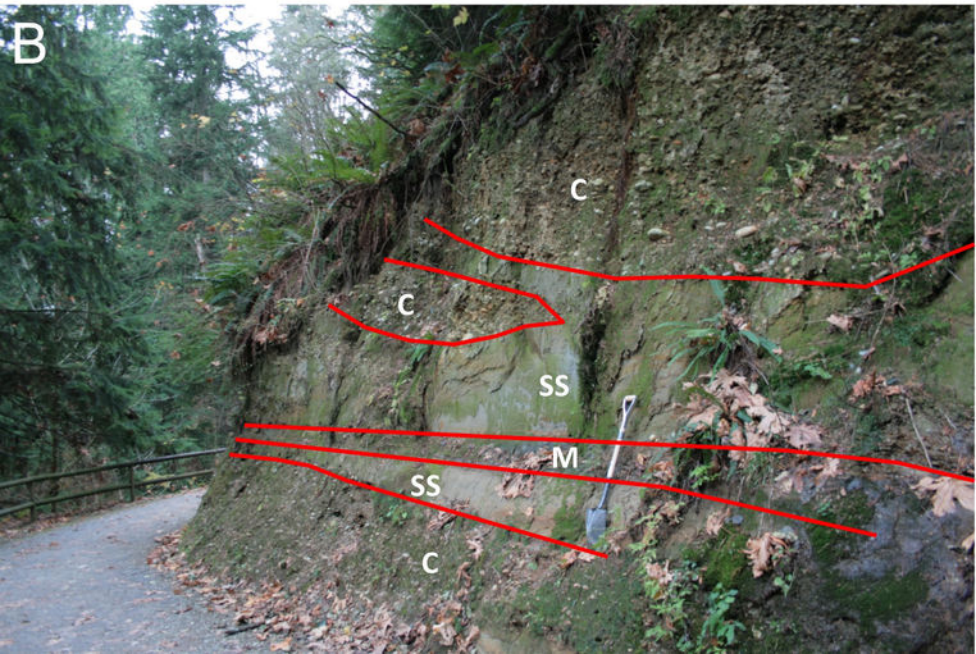
B
C
C
SS
M
SS
C

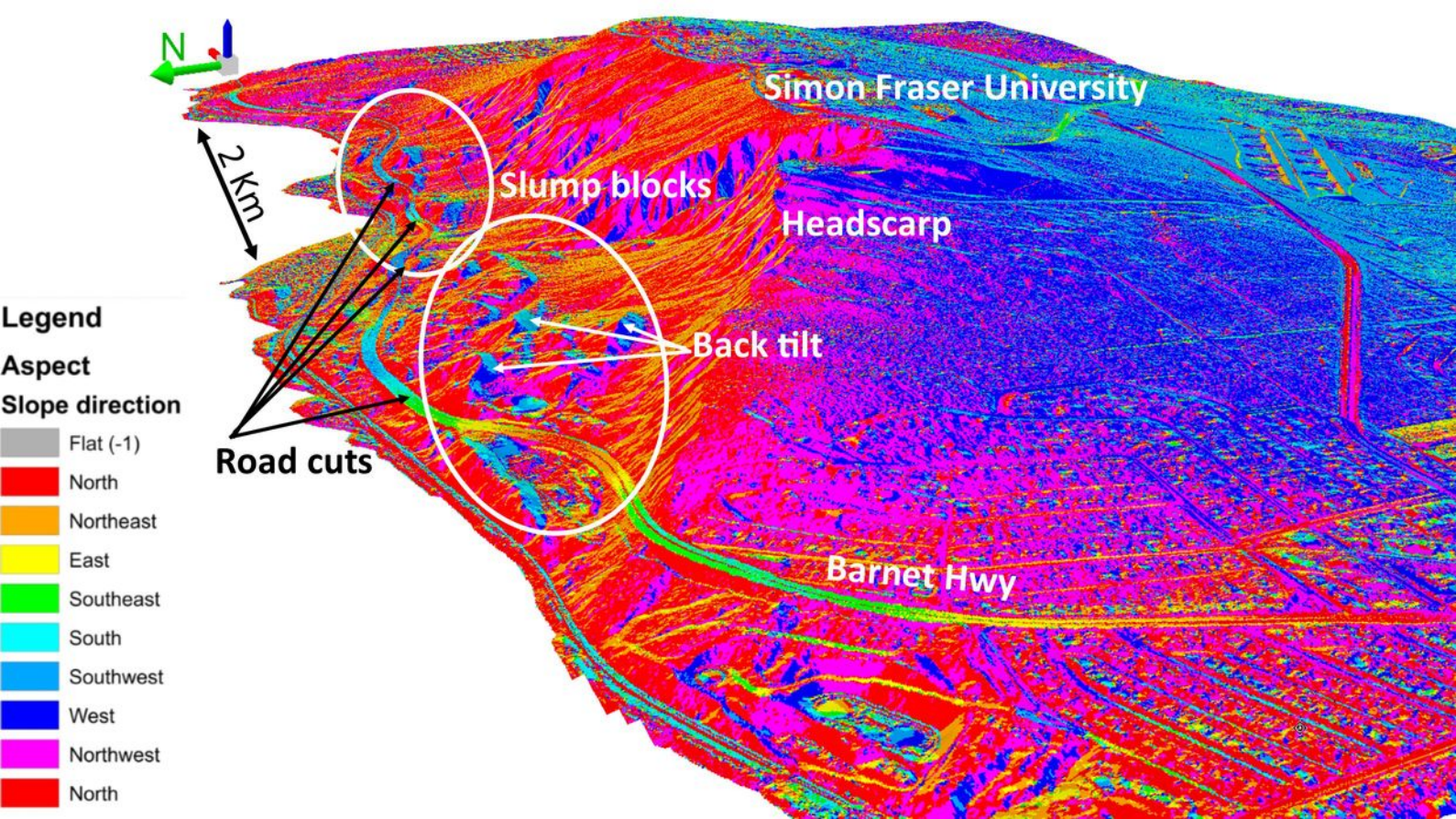
N
2 Km
Simon Fraser University
Slump blocks
Headscarp
Back tilt
Road cuts
Barnet Hwy
Legend
Aspect
Slope direction
Flat (-1)
North
Northeast
East
Southeast
South
Southwest
West
Northwest
North

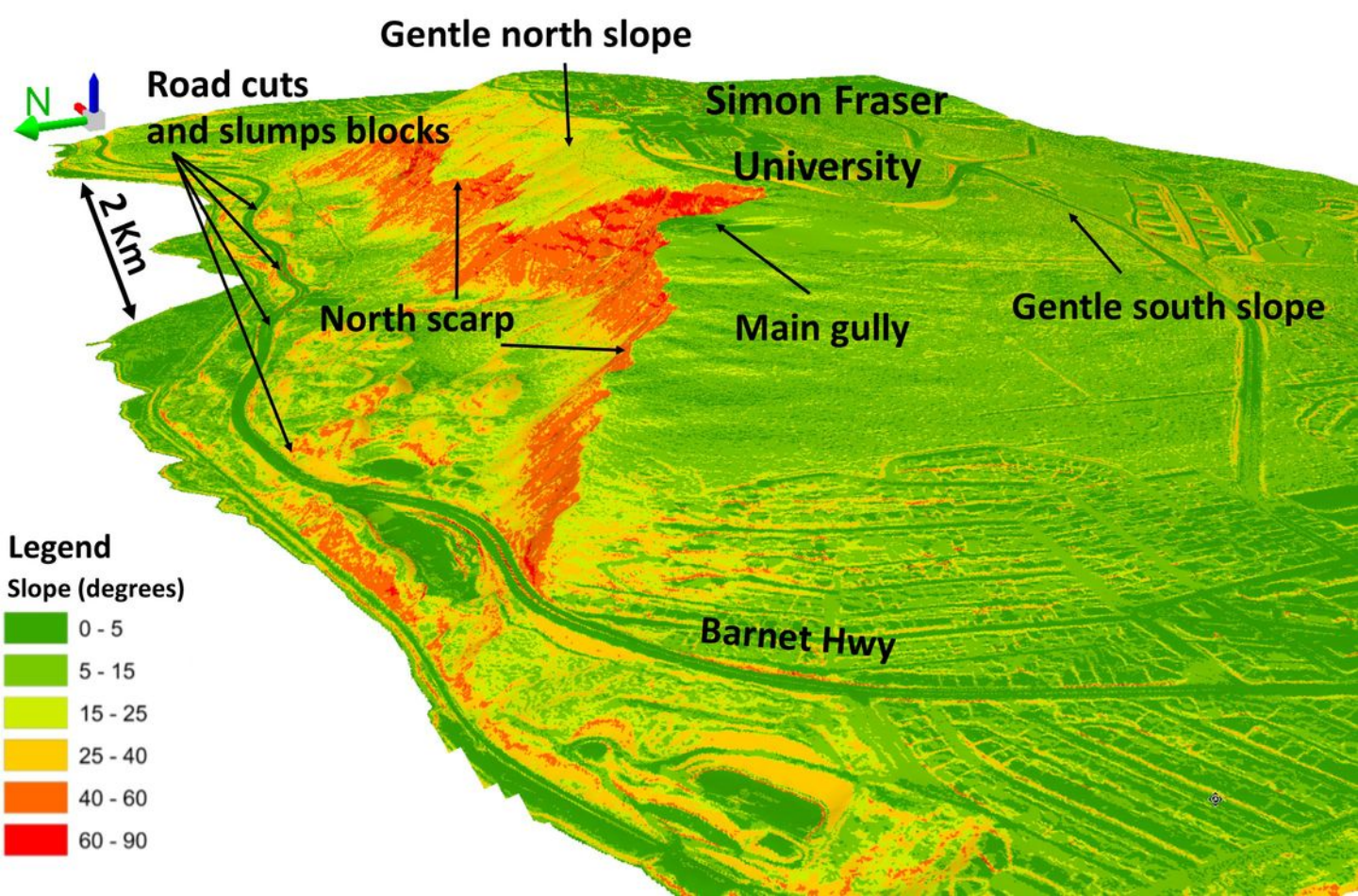
Gentle north slope
Road cuts
and slumps blocks
Simon Fraser
University
2 Km
North scarp
Main gully
Gentle south slope
Barnet Hwy
N
Legend
Slope (degrees)
0 - 5
5 - 15
15 - 25
25 - 40
40 - 60
60 - 90

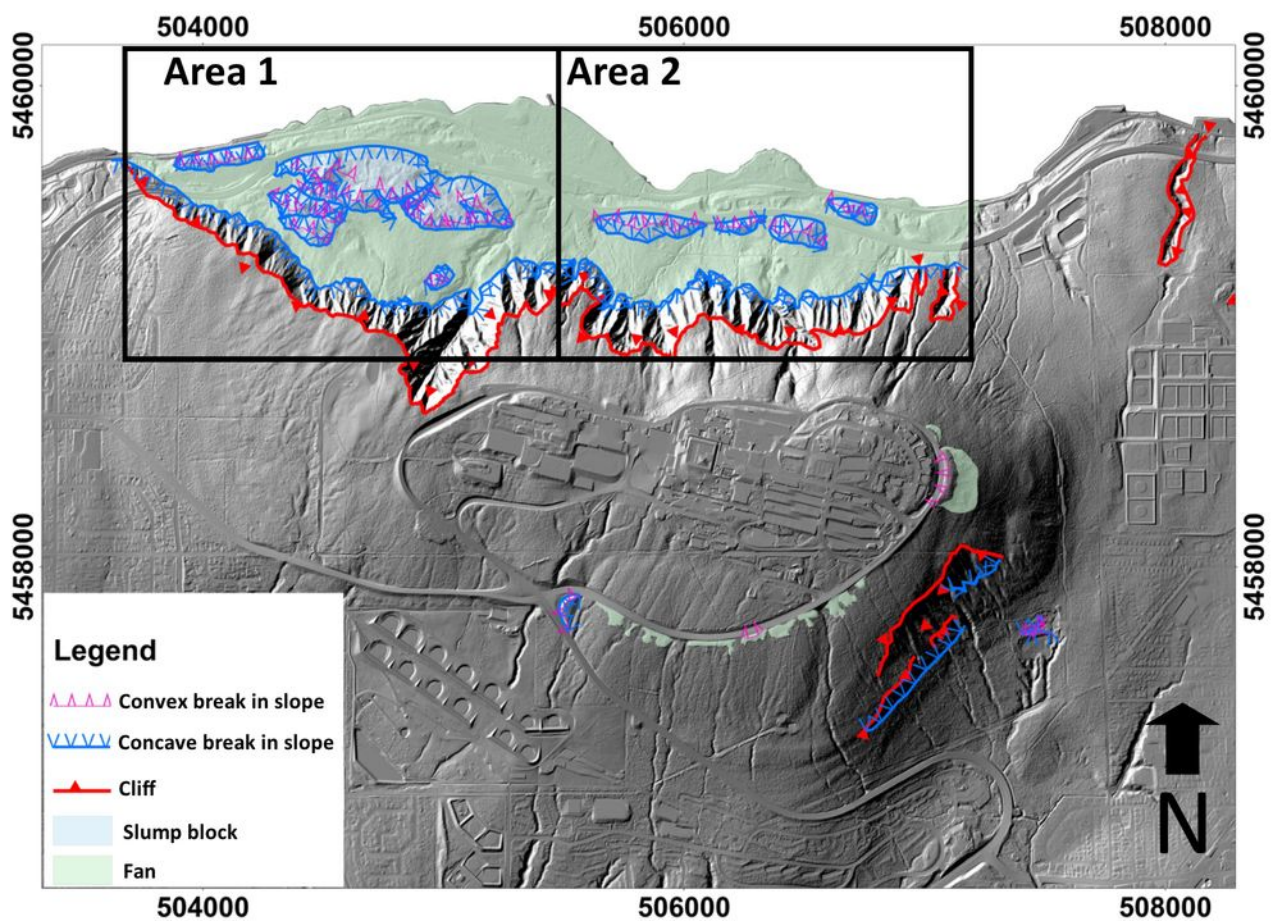
504000
506000
508000
5460000
5458000
Area 1
Area 2
Legend
Convex break in slope
Concave break in slope
Cliff
Slump block
Fan
N

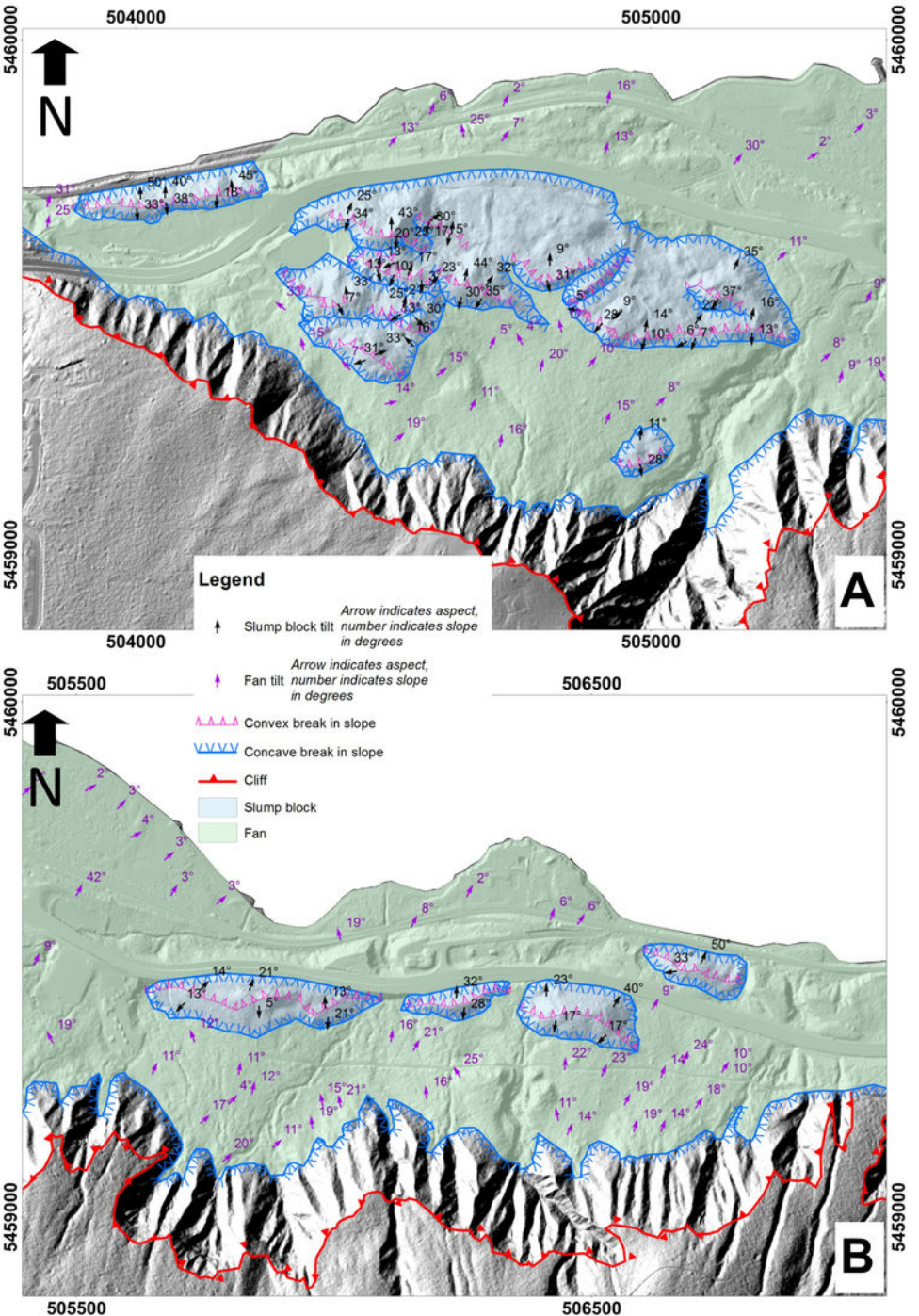
504000
505000
5460000
5459000
N
A
Legend
Slump block tilt
Arrow indicates aspect, number indicates slope in degrees
Fan tilt
Arrow indicates aspect, number indicates slope in degrees
Convex break in slope
Concave break in slope
Cliff
Slump block
Fan
505500
506500
B

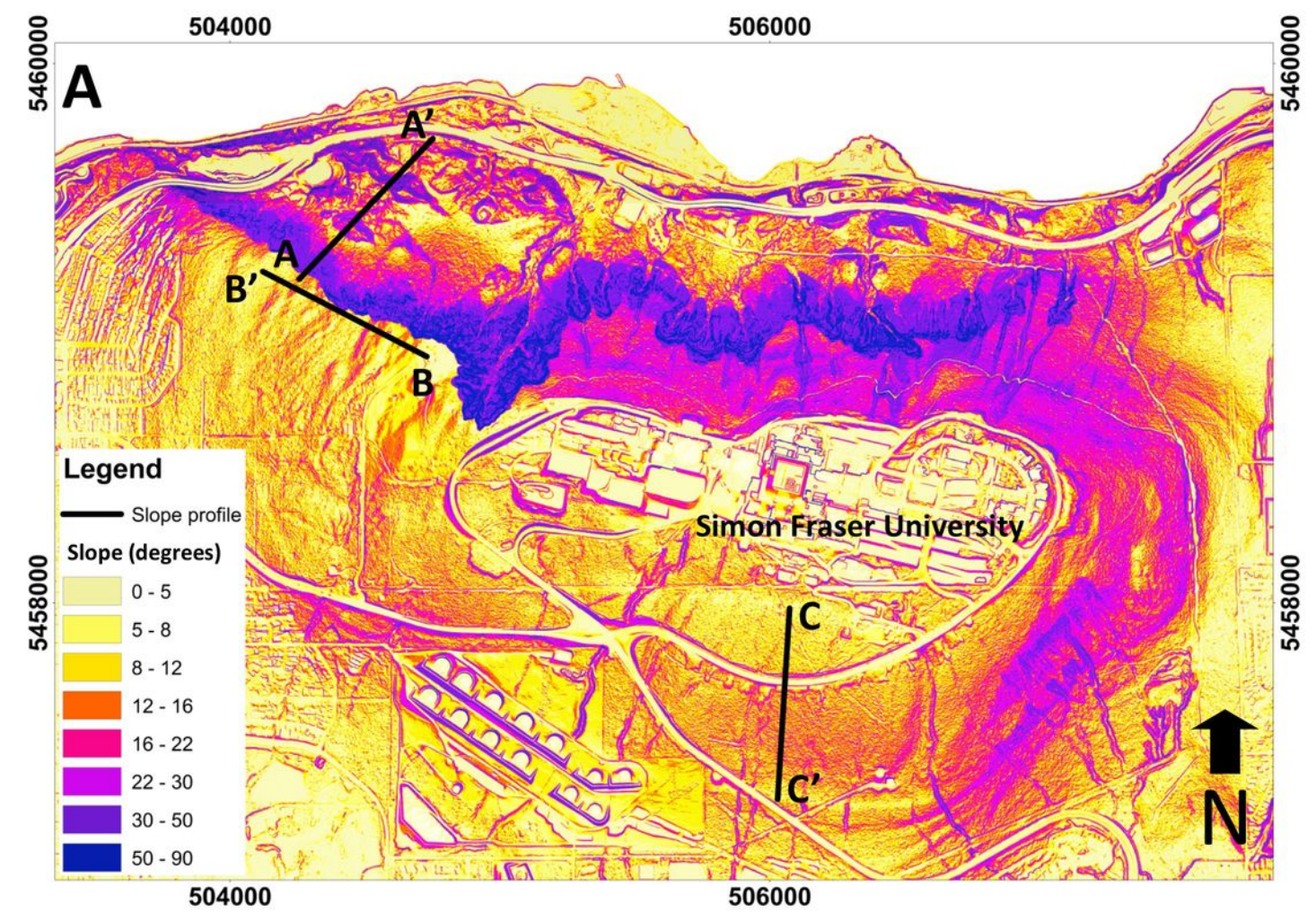
A
504000
506000
5460000
5458000
A'
A
B'
B
C
C'
Simon Fraser University
N
Legend
Slope profile
Slope (degrees)
0 - 5
5 - 8
8 - 12
12 - 16
16 - 22
22 - 30
30 - 50
50 - 90

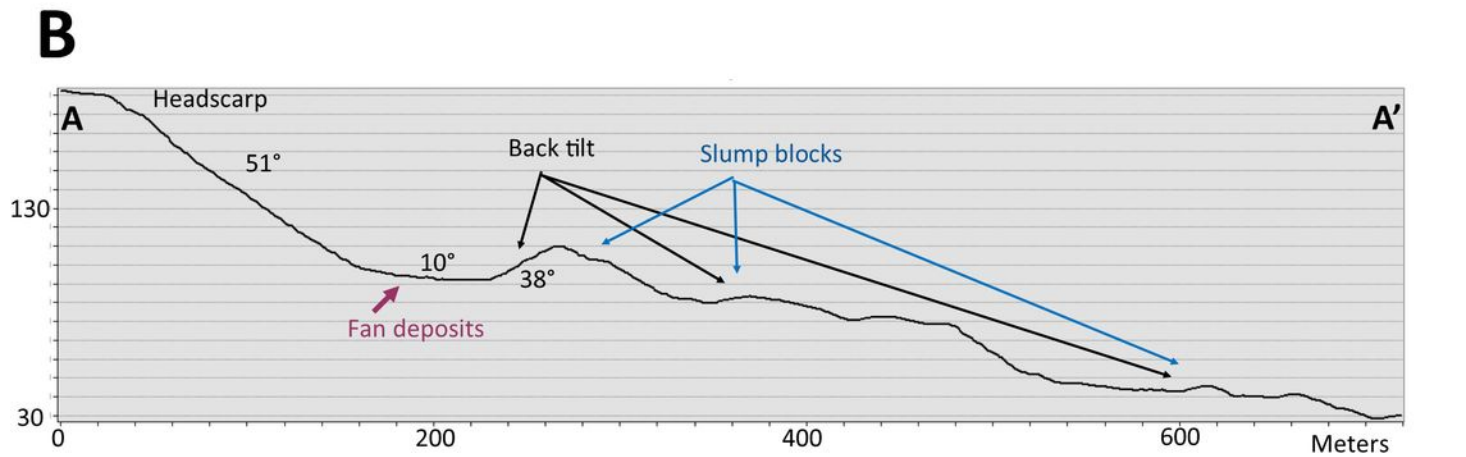
B
A
A'
Headscarp
51°
Back tilt
Slump blocks
10°
38°
Fan deposits
130
30
0
200
400
600
Meters

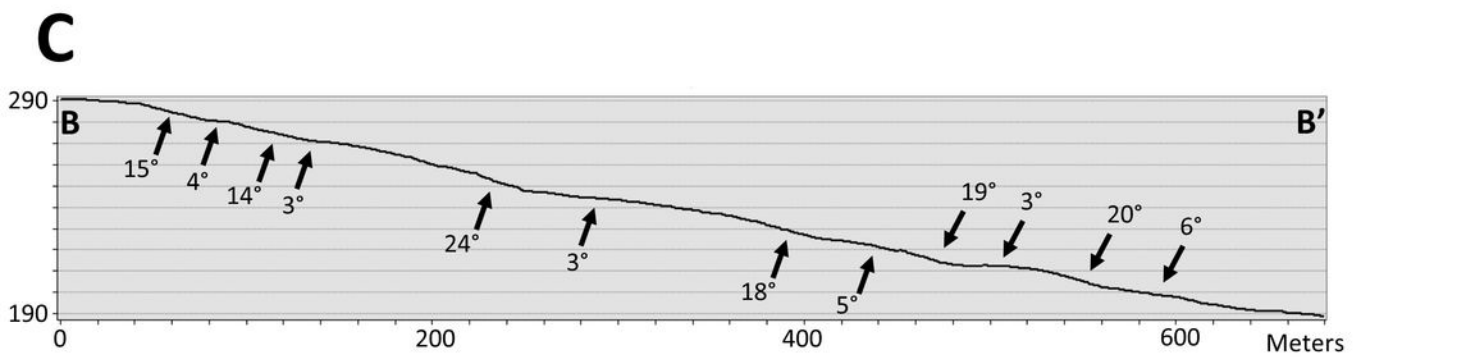
C
B
B'
15°
4°
14°
3°
24°
3°
18°
5°
19°
3°
20°
6°
290
190
0
200
400
600
Meters

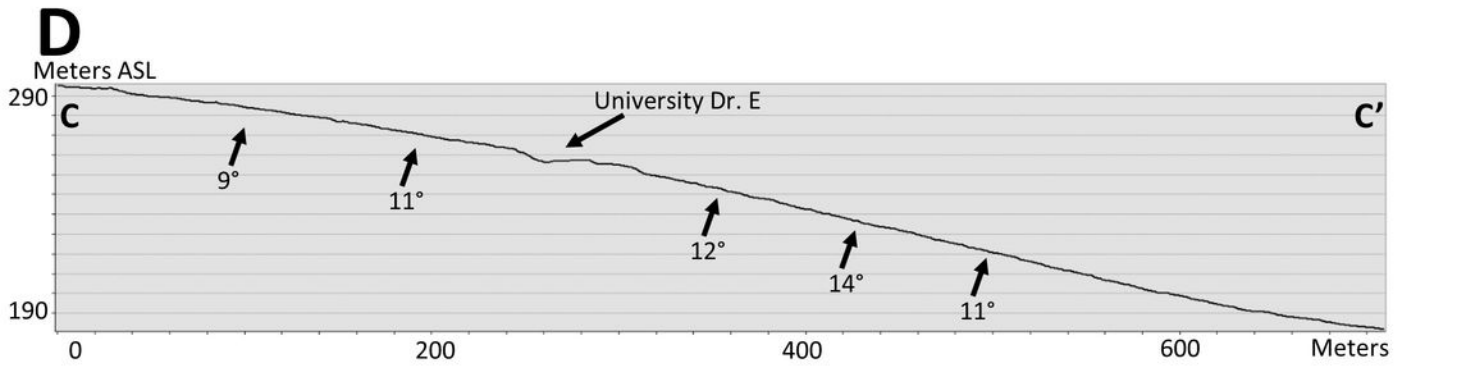
D
Meters ASL
C
C'
University Dr. E
9°
11°
12°
14°
11°
290
190
0
200
400
600
Meters

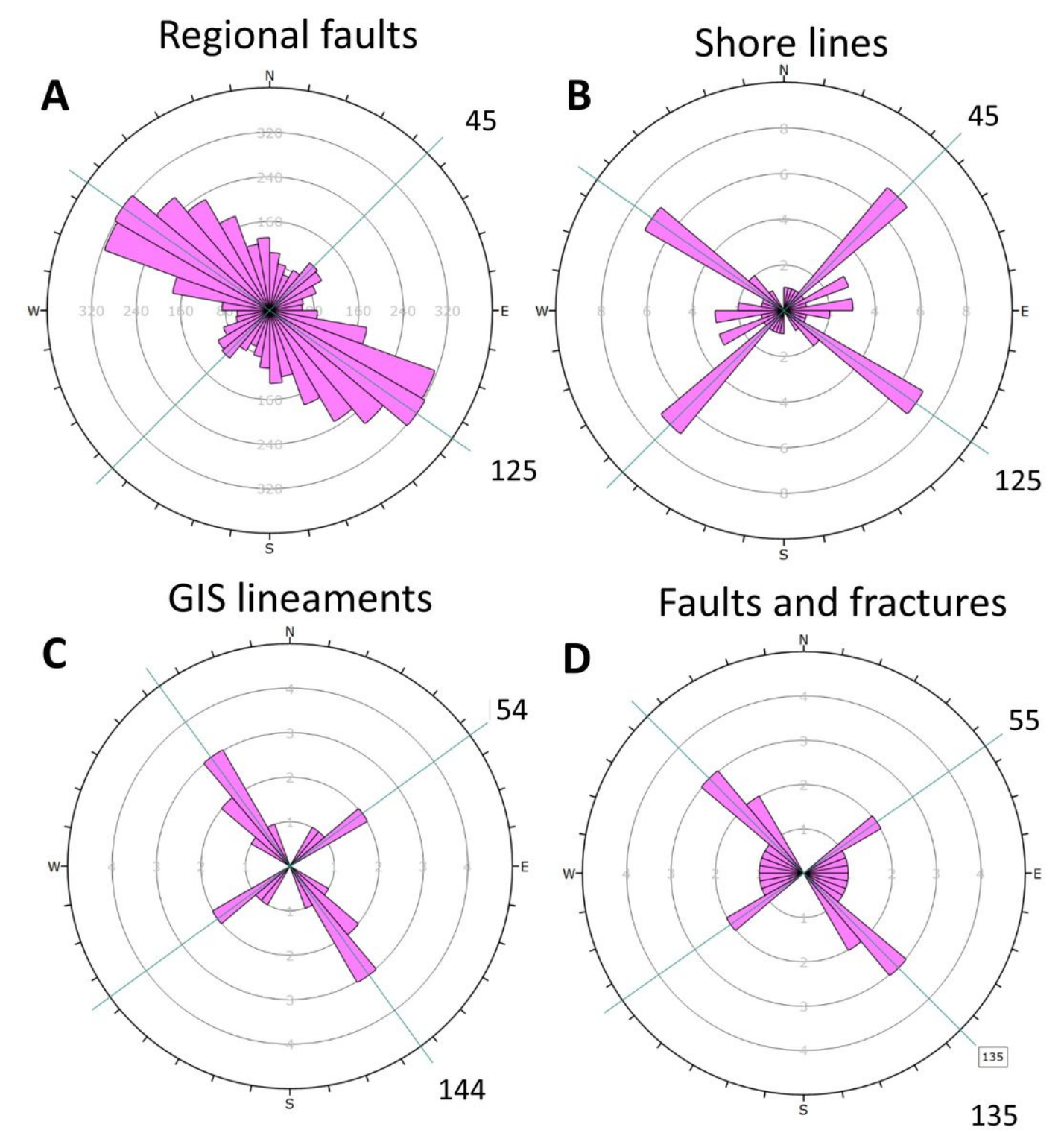
Regional faults
A
N
45
125
S
W
E
Shore lines
B
N
45
125
S
W
E
GIS lineaments
C
N
54
144
S
W
E
Faults and fractures
D
N
55
135
135
S
W
E

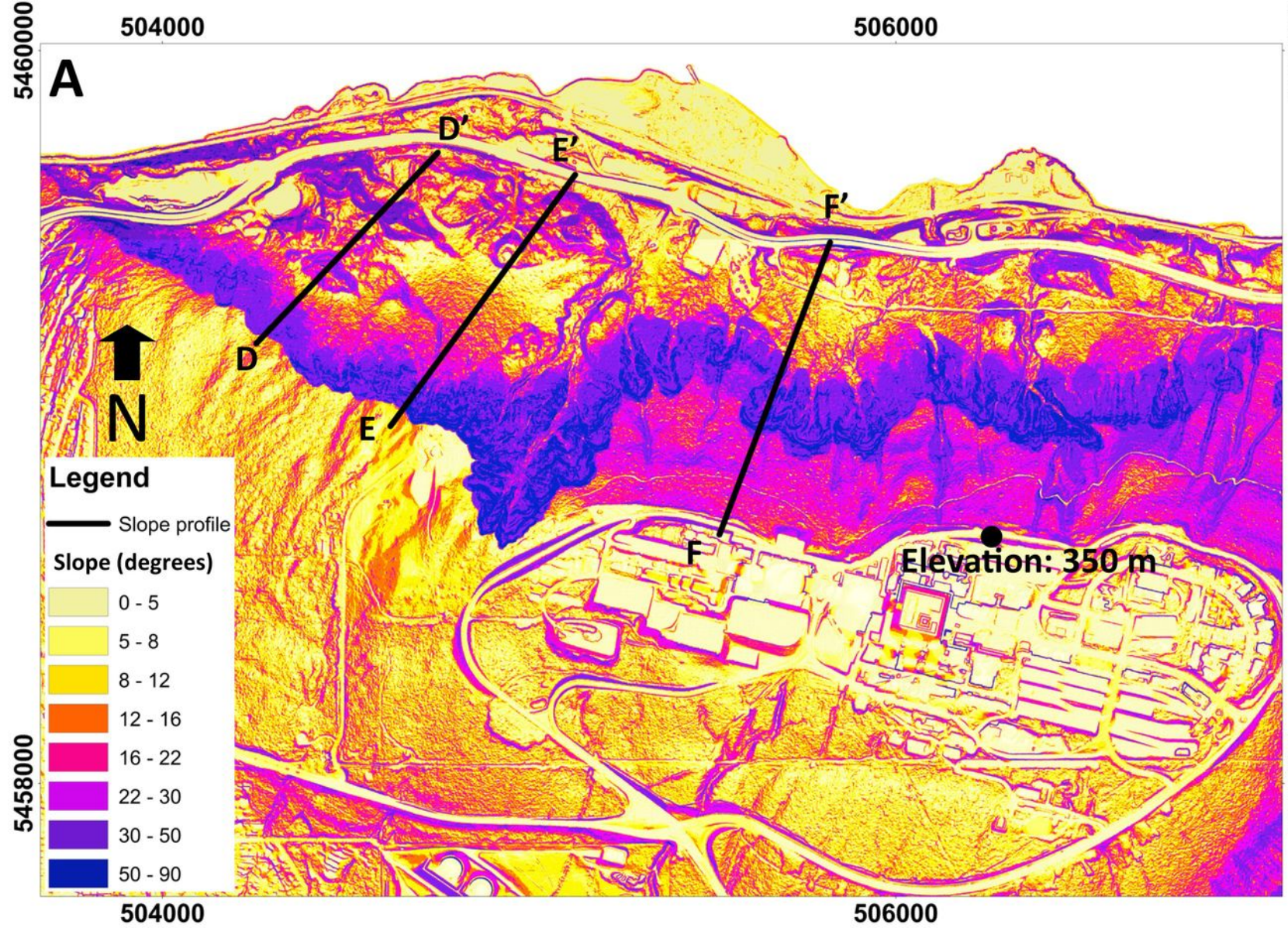
A
504000
506000
5460000
5458000
D
D'
E
E'
F
F'
N
Legend
Slope profile
Slope (degrees)
0 - 5
5 - 8
8 - 12
12 - 16
16 - 22
22 - 30
30 - 50
50 - 90
Elevation: 350 m

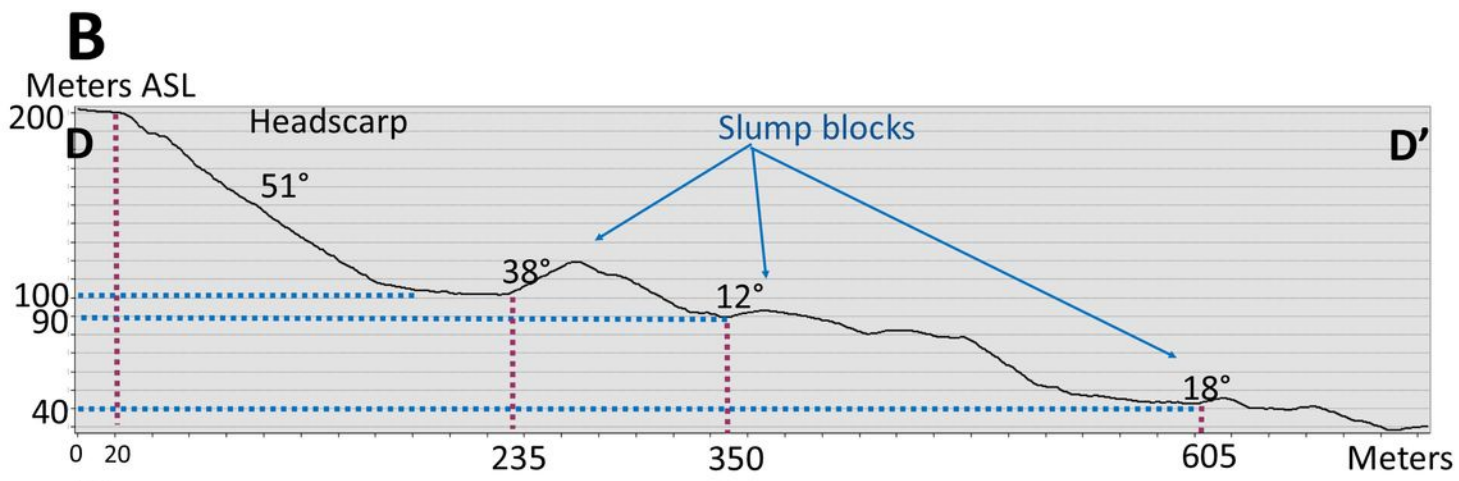
B
Meters ASL
200
100
90
40
D
D'
Headscarp
51°
38°
12°
18°
Slump blocks
0
20
235
350
605
Meters

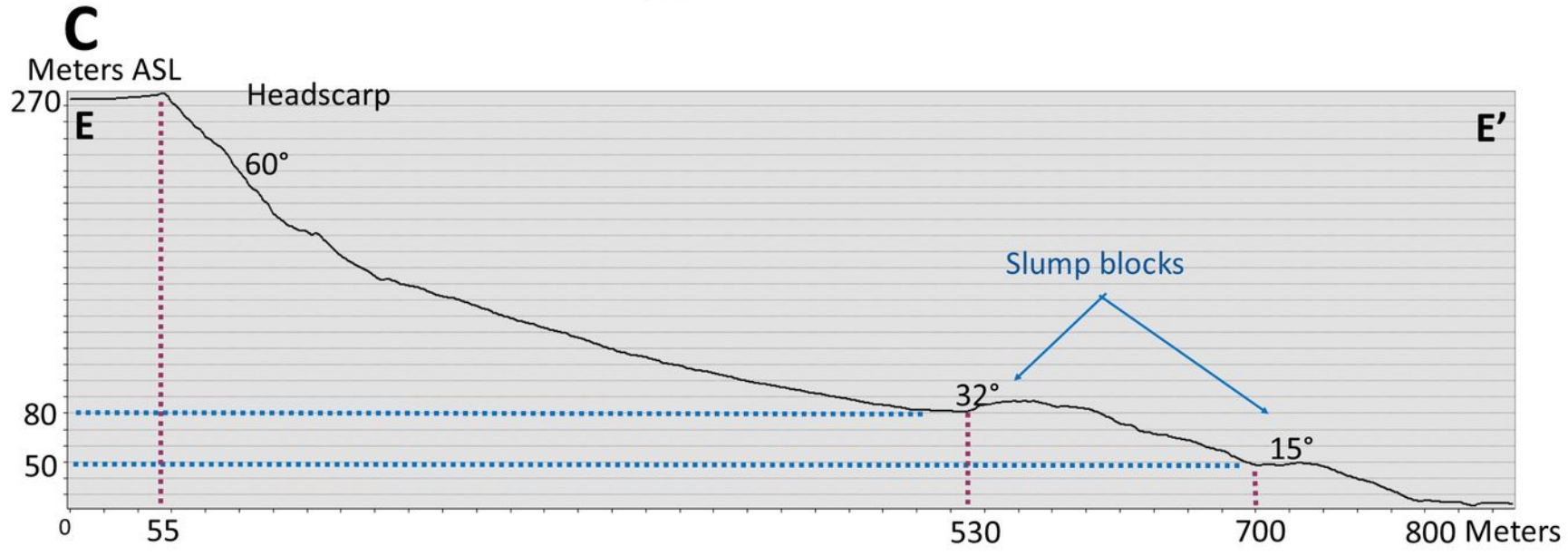
C
Meters ASL
270
80
50
E
E'
Headscarp
60°
32°
15°
Slump blocks
0
55
530
700
800 Meters

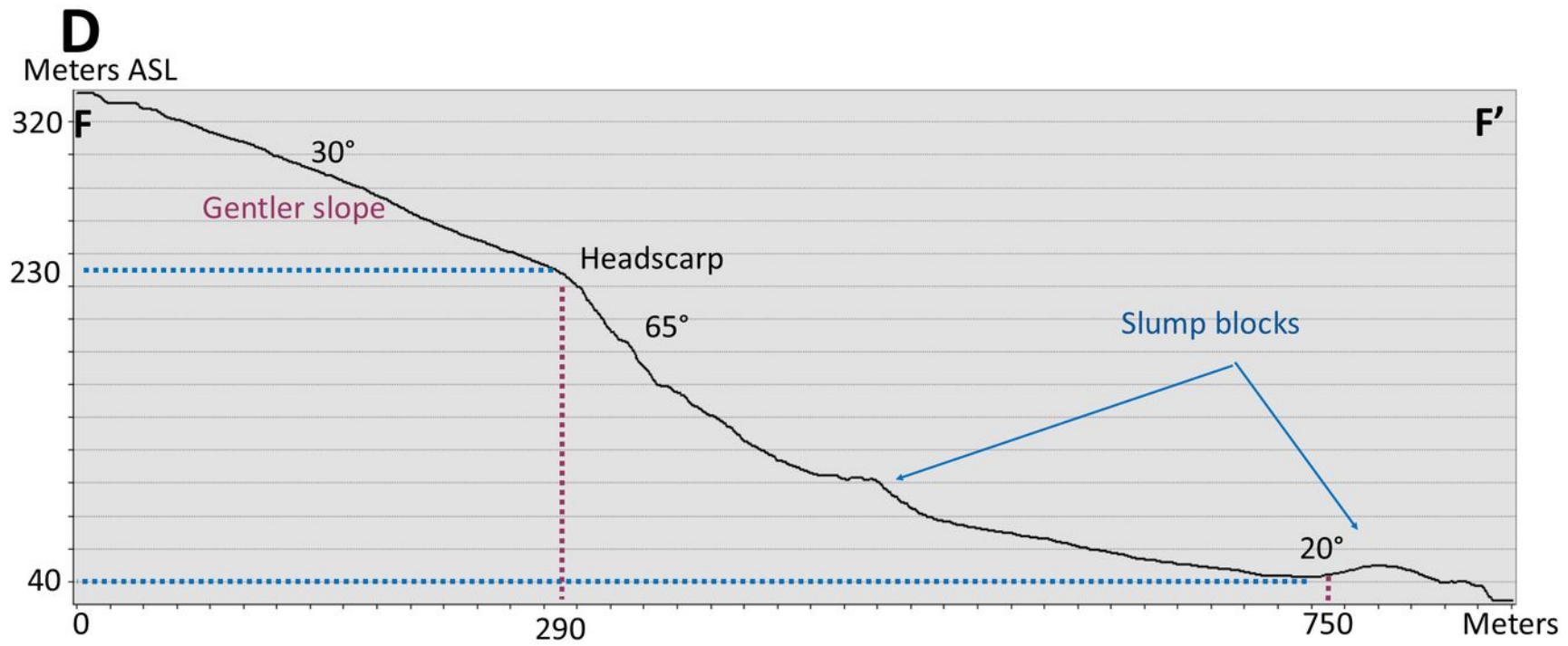
D
Meters ASL
320
230
40
F
F'
30°
Gentler slope
Headscarp
65°
20°
Slump blocks
0
290
750
Meters

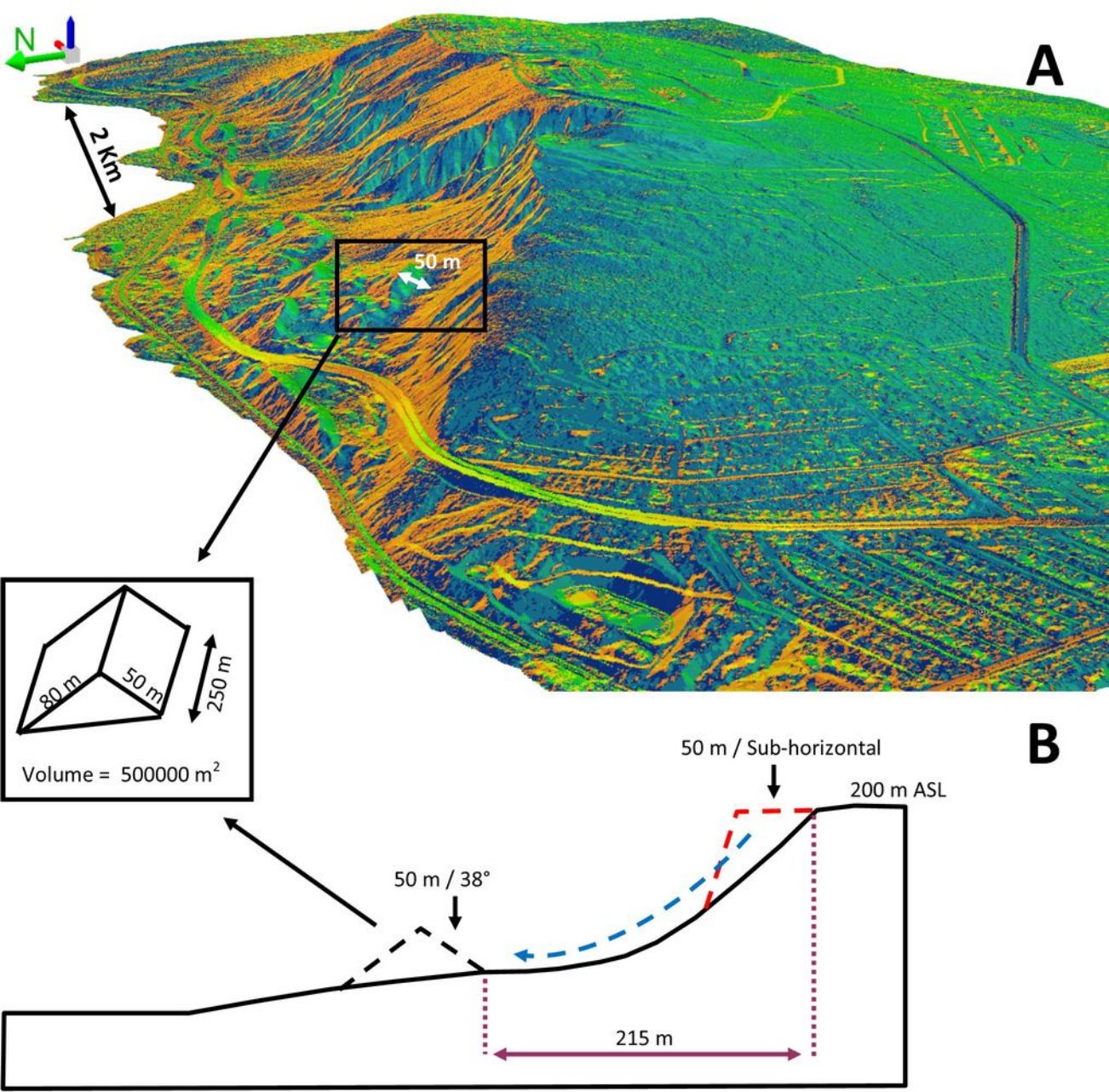
N
A
2 Km
50 m
80 m
50 m
250 m
Volume = 500000 m²
B
50 m / Sub-horizontal
200 m ASL
50 m / 38°
215 m